On the Interplay between Distributed Bulk Plasticity and Local Fault Slip in Evolving Fault Zone Complexity

Mohamed Abdelmeguid[a], Md Shumon Mia[b,c], and Ahmed Elbanna[b,d]

[a]Graduate Aerospace Laboratories, California Institute of Technology, Pasadena, CA, USA.
[b]Department of Civil and Environmental Engineering, University of Illinois at Urbana-Champaign, Urbana, IL, USA
[c]Department of Mechanical Science and Engineering, University of Illinois at Urbana-Champaign, Urbana, IL, USA
[d]Beckman Institute of Advanced Science and Technology, University of Illinois at Urbana-Champaign, Urbana, IL, USA,

[⋆]e-mail: meguid@caltech.edu

Key Points:

- Partitioning of deformation between bulk and fault contribute to seismic complexity.
- Seismic complexity and accumulation of plastic strain induce normal stress perturbations on the fault.
- Off-fault inelastic deformation result in cascading earthquake.

Abstract

We numerically investigate the role of plastic strain accumulation on the mechanical response of a planar strike-slip fault. Our models show that fault-zone strength significantly impact the ensuing sequence of earthquakes. Weaker fault zones accumulating more plastic strain promote more complexity in the seismicity pattern through aperiodic earthquake occurrences and intermittent episodes of rupture and arrest. However, if the fault zone strength is high enough, the overall earthquake sequence is characterized by periodic fault-spanning events. We find that both the fault normal stress and the fault surface profile evolve throughout the earthquake sequence, suggesting a self-roughening mechanism. Despite the significant impact of plasticity on the fault response, the width of the plastically deforming region in the fault zone is small compared to the fault length. Our results suggest a rich behavior in dynamically evolving fault zones and support the need for further high-resolution studies of the highly non-linear near-fault region.

Plain Language Summary

Why do some faults fail in large earthquakes while other faults generate smaller ones? In our computer simulation study, we explored how the strength of a strike-slip fault (where Earth's crust plates slide past each other) affects earthquake patterns. We discovered that weaker fault zones, which can stretch or squeeze more, often have more complex and unpredictable earthquake patterns, including irregular timings and smaller, clustered earthquakes. In contrast, stronger fault zones tend to have regular, larger earthquakes. Interestingly, in weaker fault zones, the geometry of the fault surface can change over time and become rougher in response to the

deformability of the surrounding rocks, suggesting a roughening of the fault surface. Although these changes significantly influence earthquake patterns, they occur in a relatively small region surrounding fault surfaces highlighting the need for expanding instrumentation closer to active faults. These findings are useful for contextualizing observed seismicity patterns and are relevant for seismic hazard studies.

1 Introduction

Geological observations of fault zones highlight a region of pervasive damage that surrounds the principal slip surfaces [1–7]. A typical strike slip fault zone may have one or more fault cores with damage features at varying length scales from fine scale distributed damage to more discrete anistropic secondary faults. In general, the distribution and intensity of damage decays away from the main fault, leading to a gradual transition from a damaged zone to intact host rock [2, 8]. Extensive studies on damaged fault zones reveal substantial differences between the mechanical properties of the inner fault zone core compared to the host rock material[9, 10]. This variation in fault zone properties was found to influence many rupture characteristics including rupture directivity [11], rupture speed , high frequency generation [12], maximum event magnitude[13], radiation patterns [14–18] and surface deformation [19].

Fault zone damage may accumulate both seismically and aseismically [1, 2, 20, 21] and is generally enhanced in the presence of geometrical complexity [22–30]. Prior studies suggest that regardless of the damage generation mechanism, the scale of damage evolution varies based on the maturity of the fault core [31]. Specifically, fault zone damage scales with fault slip up a certain threshold above which the fault zone width growth is minimal [8, 32]. Furthermore, the damage density decreases exponentially or as a power law with distance normal to the fault surface [8, 26, 33].

Fault zone damage has been studied extensively using dynamic rupture simulations [34–36] using different idealizations including plasticity theories and continuum damage mechanics as well as the limiting case of an elastic low velocity fault zone. Among the major conclusions of these studies are that the damage region contributes to a heterogeneous local stress field on the fault, acts as an energy sink increasing the total energy dissipated during dynamic rupture, and leads to generation of trapped waves that may enhance high frequency generation and influence the rupture mode. While, dynamic rupture simulations provide significant insight into the accumulation and effects of damage during earthquake rupture. Field observation indicates that damage accumulation on larger faults is associated with overprinting from multiple slip events rather than a single dynamic event. To this point, earthquake cycle simulations that are capable of modeling sequences of earthquakes are a prime candidate for the study of evolving damage profiles on a fault zone. However, due to the numerical complexity of modeling multiple earthquakes over different spatial and temporal scales, only a handful of earthquake cycle studies investigated the effect of the bulk material response, beyond elasticity [21, 30, 37–39]. In anti-plane approximation, [38] utilized a combined finite element spectral boundary integral scheme (FEBE) to investigate the effects of the bulk yield strength on the overall sequence of the earthquake and asesismic slip and the evolution of inelastic strain. In that study, they demonstrated that the partitioning between off-fault deformations and fault slip could lead to a complex sequence of seismicity. However, within that study, the role of pressure-dependent rock strength was neglected. Recently, Abdelmeguid and Elbanna demonstrated, in the context of 2D plane-strain approximation, that there is a feedback mechanism between the evolution of plastic strain in the bulk and mean stress which in turn influences the pressure-dependent yield strength and subsequent generation of plastic strain [21]. Accordingly, it still remains to be investigated whether the spatio-temporal clustering observed in the anti-plane model would persist in the context of in-plane deformations, and what role the feedback between mean stress and inelastic strain accumulation plays in fault zone maturity.

In this paper, we focus on aspects related to the co-evolution of seismicity and off-fault viscoplastic bulk rheology. We consider the 2D plane-strain approximation as a minimal model that enables us to study the role of pressure-dependent plasticity. We use a hybrid finite element spectral boundary integral framework, FEBE, which accounts for the full inertia effect during the seismic phase and enables accurate near field truncation of the wave field. We study the evolution of the sequence of earthquakes and aseismic slip for different choices of bulk strength and implications for event size distribution, partitioning of deformation, stress heterogeneity, and fault surface evolution. We outline the setup of the model and summarize the main results in the next section

2 Model Description

We consider a planar horizontal fault, with a right-lateral sense of motion, the frictional behavior is governed by rate-and-state friction under a 2D plane strain approximation. The fault is bisecting an unbounded elastic-visco-plastic domain with homogeneous elastic properties as shown in Figure A1a. The fault consists of a central velocity weakening patch surrounded by two velocity strengthening patches and is being loaded from both ends by a constant plate loading rate as shown in Figure A1b. The initial prestress σ_{ij}^{o} shown in Figure A1b is assumed to be uniform.

The bulk is initially assumed to be linear elastic. We use pressure-dependent Drucker-Prager (DP) plasticity to describe the inelastic bulk response beyond the onset of yielding. The DP yield surface is parameterized by two parameters: the angle of internal friction ϕ and cohesion c. We assume a non-associative flow rule and Perzyna type viscous regularization. We vary the value of the cohesion parameter c to explore the effect of fault zone strength on the evolution of seismicity and near fault stresses and deformations. We implement normal stress regularization on the fault surface following Prakash-Clifton law that ensures the fault local frictional strength is a function of the history of the normal stress on the fault and eliminates any spurious unstable modes that may emerge due to rapid variations in the instantaneous value of the normal stress [40–42].

We use the FEBE framework presented in [21, 43] to explore the co-interplay between localized fault slip and distributed bulk inelastic deformations through long sequences of earthquakes and aseismic slip (SEAS). FEBE is a hybrid finite element spectral boundary integral scheme. Spatially, FEBE adopts a domain decomposition approach where the near fault region that includes the potentially nonlinear material response is discretized using the finite element method. The exterior half spaces beyond the near fault region are assumed to be linear elastic and homogeneous and are thus described by a spectral boundary integral formulation. The fault zone and the exterior half spaces are coupled through the enforcement of continuity of traction and displacement at their interfaces. The local nature of near-fault nonlinearities ensures that the width of the discretized region W_s (shown in Figure A1b) is usually much smaller than the total domain length L_T. The FEM domain size is selected such that the discretized domain contains all the off-fault plasticity. For planar faults previous studies on dynamic fracture with off-fault plasticity suggest that the extent of the plastic zone is proportional to the process zone size, this estimate guides our initial choice of W_s [34, 44].

Temproally, FEBE implements an alternating quasi-dynamic scheme, to resolve interseismic slow deformation while neglecting inertia effects, and a fully dynamic scheme, to resolve rapid seismic periods while accounting for fully inertia effects. The switch between the two schemes is determined by a velocity threshold. More details about the numerical algorithm may be found in Abdelmeguid and Elbanna 2022 [21]. The values of the different parameters used in the model are summarized in Table A1

3 Results

3.1 Spatial and Temporal Complexity

Figure 1a-d shows the temporal evolution, measured in simulation time steps, of the slip rate along the fault surface during the earthquake cycle for four different cases with decreasing cohesion. As discussed earlier, cohesion contributed to bulk strength. The lower the bulk cohesion, the more prone to yielding the fault zone becomes. We observe that as bulk strength decreases, spatio-temporal complexity of the earthquake sequence emerges. This is evident in the transition from periodic events with slight variation in the nucleation characteristics, at $c = 35$ MPa, to intermittent earthquake with strong rupture segmentation and temporal clustering, for $c = 22$ MPa. Similar to observations in the antiplane deformations [38] plasticity accumulation around the rupture tip may result in the pinning of the rupture which in turn leads to local rupture arrest and spatial segmentation of coseismic slip. For all four cases shown here, the pattern of seismicity varies. We show that based on the choice of cohesion the ensuing seismic cycle can include partial ruptures, slow events, and intermittent episodes of earthquakes. This complexity is a direct consequence of the competition between on-fault and off-fault deformations.

In the case of $c = 35$ MPa, most of the events within the sequence are periodic and through-going with shifts in the nucleation site. In the cases of $c = 30$ MPa, and $c = 26$ MPa the sequence of events are quasi-complex. For the case of $c = 30$ MPa, seimcity converges to a sequence of doublets: a partial rupture followed by a through-going rupture and this combination keeps repeating. For the case of $c = 26$ MPa, the spatio-temporal complexity increases. However, the complex pattern appears to approximately repeat itself over longer time scales. The end member case with $c = 22$ MPa shows no distinguishable pattern and no diminished complexity with time.

To demonstrate the temporal complexity induced by plastic strain accumulation in Figure 1e we compare the time history of the peak slip rate for the two cases of $c = 35$ MPa and $c = 22$ MPa. We observe significant differences between the two cases in terms of the inter-event time, peak slip rates, and the emergence of foreshocks and aftershocks. Figure 1f focuses on the seismic activity leading up to a number of mainshocks (marked by the stars) in the case of $c = 22$ MPa. Here, we define the mainshock as an event with peak slip rate exceeding 0.1 m/s. We observe that the slip rate on the fault surface doesn't not change gradually, but rather through a burst of microseismicity leading up to the mainshock. This temporal complexity results from plasticity accumulation and stress redistribution which controls the growth and arrest of these transients. Zoomed-in panels in Figure 1f expand on this observation and by focusing on the few seconds to minutes around the time of occurrence of the main shock. What appears as a single spike in Figure 1e on the scale of years is indeed a complex sequence of clustered seismic activity with intermittent episodes of earthquakes characterized by closely spaced bursts of accelerated motion associated with spontaneous nucleation and arrest of the rupture front multiple times.

To further quantify the effect of plastic strain accumulation on seismicity pattern, we analyze the variability in some of the statistical characteristics of the seismic sequence with variations in the bulk strength. For example, Figure 1g-j shows the distribution of recurrence interval for each of the four values of the cohesion parameter investigated here. We observe that the choice of bulk strength has significant implications on the clustering of seismicity. At higher cohesion, the events are periodic in time with uniform interevent time (year). As the yield stress decrease, we observe a shift in the recurrence interval toward interevent times that are orders of magnitude smaller. Eventually, the recurrence interval distribution as shown in Figure 1j transitions to an almost bimodal distribution with a heavy tail that spans time scales from seconds to days. This transition is characteristic of the emergence of seismic swarms.

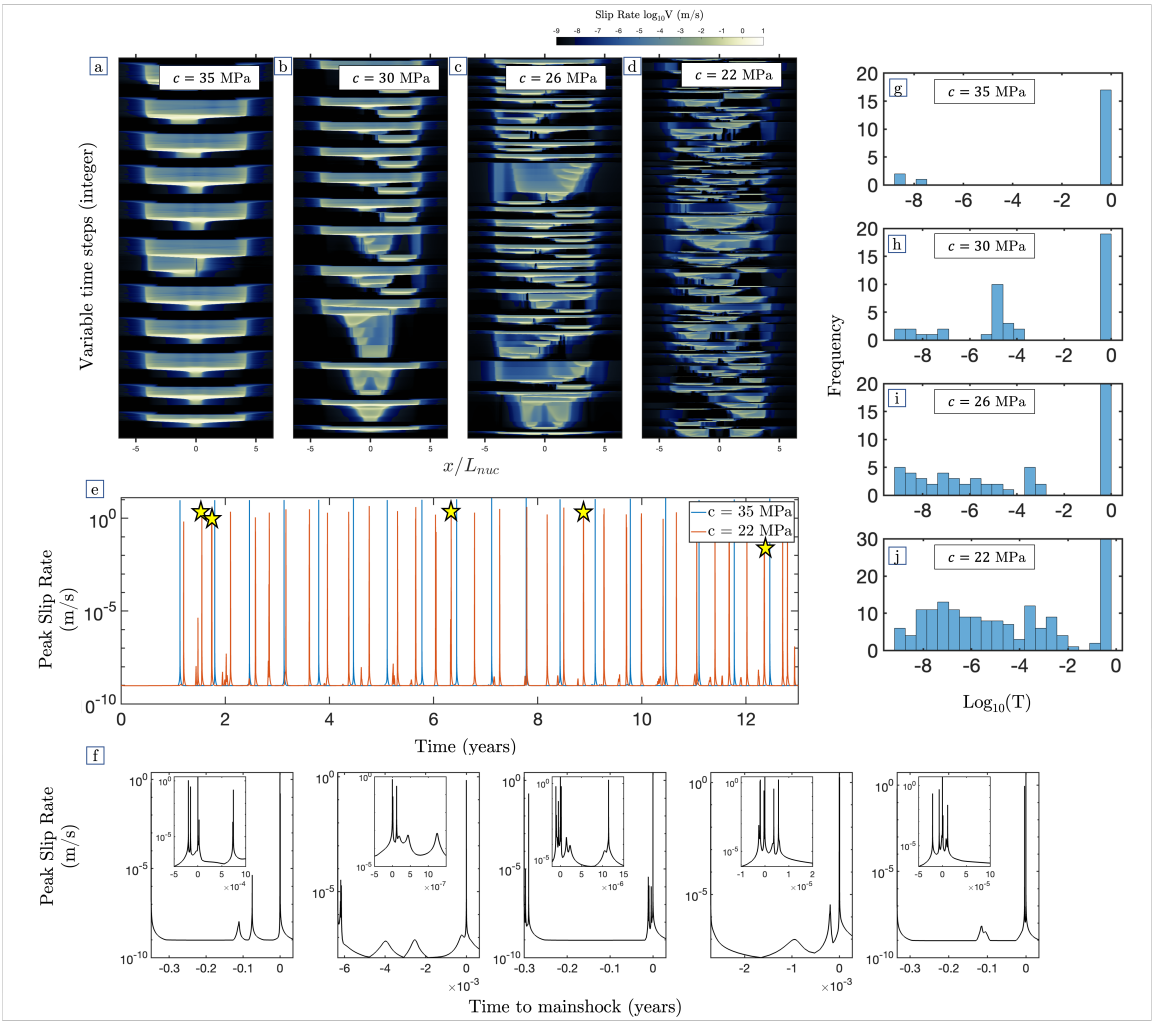

Figure 1: **Sequence of earthquakes and aseismic slip on a 2D in-plane rate-and-state fault.** (a-d) slip rate evolution with viscoplastic rheology illustrating increasing seismic complexity from periodic cycles to aperiodic sequence with segmented and partial ruptures as cohesion is reduced. (e) time history of the peak slip rate comparing $c = 35$ MPa with $c = 22$ MPa showing emergence of foreshocks and overall changes in recurrance pattern. (f) Time history panels showing foreshock patterns prior to mainshocks for several events highlighted by a yellow star in panel e. The zoomed in panels show individual event complexity. (g-j) Frequency distribution of interevent times highlighting the clustering behavior with reduction in bulk strength.

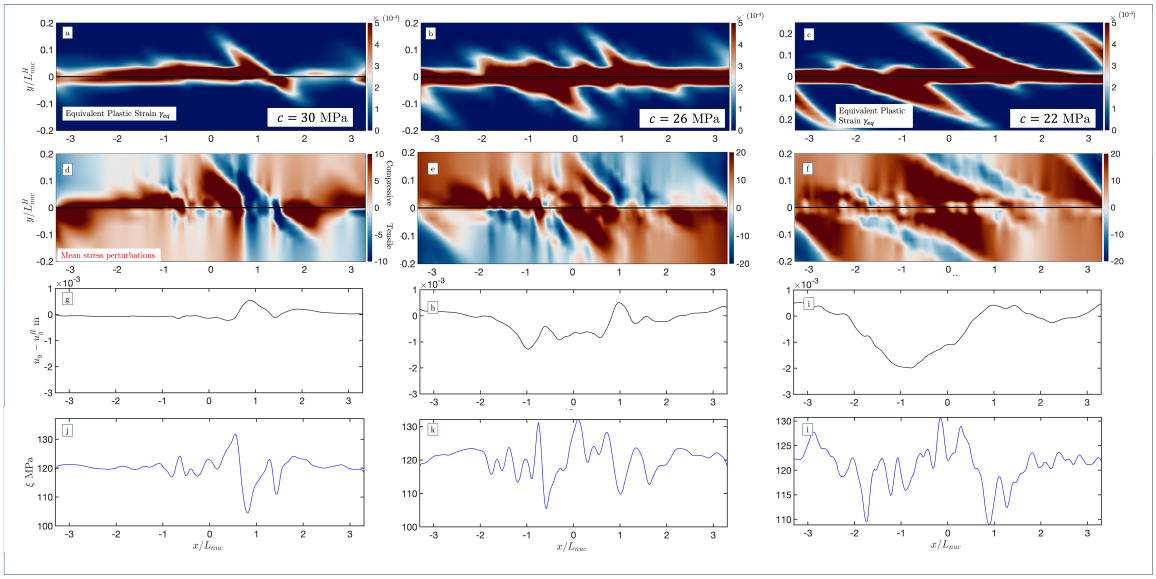

Figure 2: (a-c) The magnitude and extent of the equivalent plastic strain for three different cases of bulk cohesion c = 30, 26, and 22 MPa at the end of the simulation showing varying patterns of accumulation based on the choice of bulk strength. (d-f) The mean stress distribution within the fault zone at the end of the earthquake cycle illustrating different evolution patterns based on the accumulated plasticity and seismic compleixty. (g-i) The fault surface profile without the rotational component at the end of the cycle showing the emergence of short wave length fluctuations associated with fault zone structure evolution. (j-l) Associated changes in the normal stress on the fault demonstrating variations despite the planarity of the fault.

3.2 Evolution of Stress and Fault Structure

Simulations of single earthquakes demonstrate that the accumulation of plastic strain follows a specific pattern that is dictated by the choice of the angle of maximum compressive stress [44]. For the choices of $\Psi = 45°$ the expected pattern of co-seismic plasticity is a fan-like distribution within the extensional quadrant of the bulk, defined by the sense of motion of the rupture front. In our analysis of sequences of earthquakes and aseismic slip, we instead observe a deviation from this expected pattern. Figure 2a-c show that at the end of the seismic sequence, the inelastic strain distribution is more broadly distributed in the near-fault region and accumulates on both sides of the fault. As discussed in [45], in addition, to rupture directivity, the accumulation of plastic strain in SEAS models is dictated by two other mechanisms. First, aseismic deformations induce changes in the mean stress field σ_m which influence the yield surface and create regions with lower mean stress that could favor plastic strain accumulation in subsequent dynamic ruptures. Also aseismic deformations may generate their own plasticity if the quasi-static stress concentration associated with the creeping fronts become large enough. Second, plastic strain accumulation causes residual mean stress changes. Specifically, mean stress becomes more compressive in regions where plasticity accumulates on the extensional side [44]. However, changes in mean stress alters the yield strength which in turn impacts the potential for subsequent plastic strain accumulation. As a result, there is a correlation between plastic strain distribution and mean stress evolution. Furthermore, the mean stress field evolves, throughout the cycle, into a strongly heterogeneous distribution with alternating pockets of tensile and compressive perturbations relative to the initial mean stress value as shown in Figure 2d-f.

The magnitude, extent, and spatial distribution of the plastic strain depend on the fault zone strength as shown in 2a-c. As cohesion decreases, the width of the plastic zone increases and the magnitude of plastic strain becomes higher. This also correlates with larger variations in the mean stress that extend over larger distances away from the fault as shown in 2a-c. Importantly,

though, we observe that the width of the plastic zone in all cases is substantially smaller than the overall fault length and is on the order of a fraction of the nucleation zone size with a maximum extent of $0.2L_{nuc}$ for $c = 22$ MPa, which is approximately 3% of the total fault length. It is also important to note that the region with the most extensive plasticity accumulation is even smaller. This suggests that the implications of near fault plasticity on seismicity and stress evolution is significant despite the limited spatial extent and motivates further high resolution studies in the extreme vicinity of fault surfaces to characterize such inelastic processes.

Figure 2g-i illustrates the fault profile at the end of the simulation corresponding to different values of bulk cohesion. The fault profile is given by the magnitude of the transverse displacement u_y computed at the fault surface $y = 0$. For a homogeneous linear elastic medium, one expects a planar fault undergoing shear rupture to only rotate but remain primarily planar. The inelastic bulk rheology, however, leads to the emergence of partial ruptures due to the abrupt pinning of ruptures as well as stress heterogeneity. This results in the development of short wavelength undulations in the fault profile as shown in Figure 2g-i. To capture the variation in fault geometry in Figures 2g-i we only show the fault profile relative to overall fault rotation u_y^R. The fault rotation is computed by linearly fitting a displacement profile between the displacement at the right and the left ends of the VW patch of the fault. The magnitude and distribution of the undulations, referenced above, vary based on the choice of cohesion. Specifically, we observe that for lower bulk strength, the undulations are more pronounced. They have larger amplitudes and vary over shorter wavelengths. On the other hand, for higher cohesion (e.g. $c = 30$ MPa), the fault profile, corrected for global rotation, remains almost falt. The undulations evolve throughout the cycle and contribute to the evolution of stress fields within in the near-fault region. The magnitude of these undulations is comparable to field observations[46]. This suggests that bulk plasticity, and possibly other inelastic processes, may provide a self-roughening mechanism for faults, that has been largely understudied, even in the absence of initial roughness. Indeed, the role of pre-existing fault roughness has been previously highlighted in the development of earthquake cycle and stress heterogeneity [47]. While we have not explored the role of the fault surface evolution on the slip dynamics explicitly, which requires solving the governing equations in the updated geometric configuration at each time step, the observed dynamic self-roughening mechanism is expected to contribute to the complexity of the seismic cycle, and dynamic rupture propagation [30, 34, 47, 48]. This observation suggests it might be important to consider the role of geometric nonlinearity (i.e adapting geometries) in models of sequences of earthquakes and aseismic slip.

Tied to the evolution of the fault surface profile, Figure 2j-l shows the end results of a corresponding evolution in the regularized normal stress ξ along the fault surface. The spatial variation in the normal stress is attributed to the combined effect of the emergence of short wavelength undulations and the nonuniform accumulation of plastic strain that cause different sides of the fault to deform differently in the fault normal direction. Although the fault surface is assumed to be initially planar, the normal stress heterogeneity emerge spontaneously and evolve throughout the sequence of events. However, the characteristics of this heterogeneity depend on the bulk strength and the cohesion value. Specifically, lower bulk strength enables shorter wave length variation in the spatial distribution of the normal stress. The peak value of the normal stress, however, is similar for all three cases.

To further understand the temporal evolution of fault zone plasticity based on the choice of bulk strength, Figure 3a-c illustrates the time history of the average plastic strain evolution in the near-fault region for three cases of decreasing cohesion $c = 30$, 26, and 22 MPa. As expected, the magnitude of the average equivalent plastic strain increase with decreasing bulk strength. Similarly, we observe that the plasticity accumulated during the aseismic portion of the earthquake cycle also increases with decreasing bulk strength. Initially, during the early stages of the cycle, aseismic accumulation occurs rapidly, and then increases slowly throughout the cycle. Furthermore, we observe that the partitioning of plastic strain between the coseismic

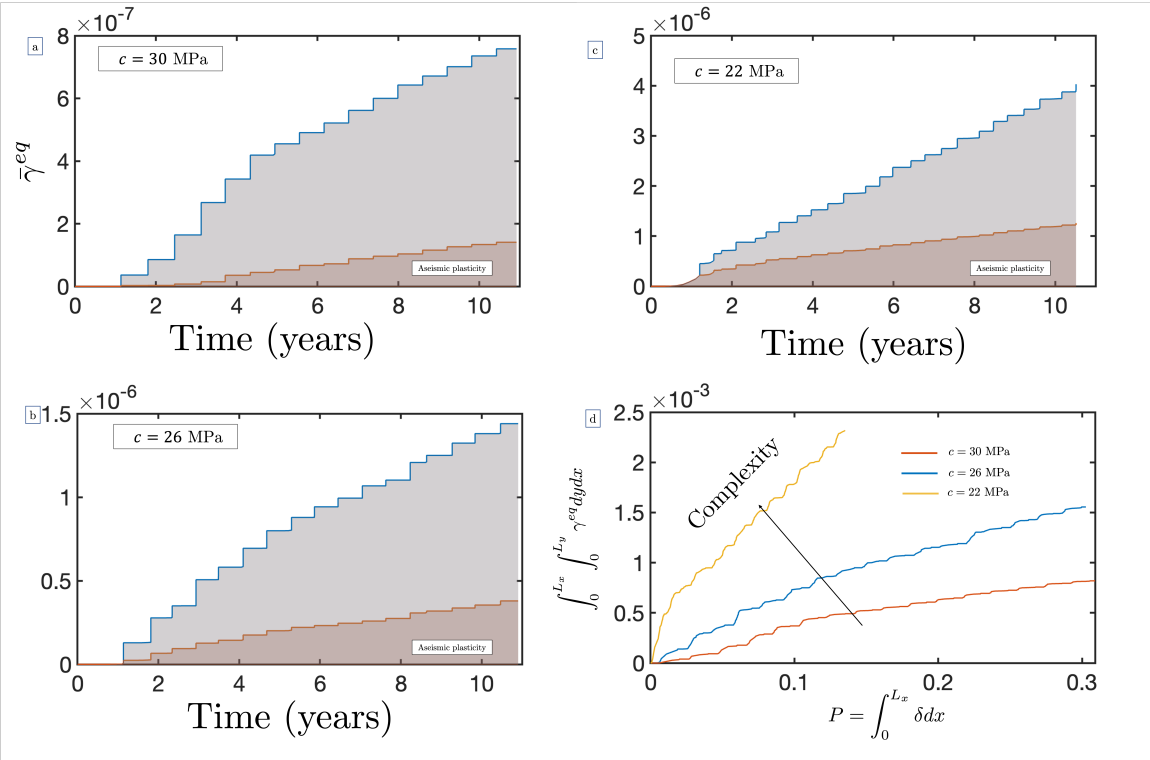

Figure 3: (a-b) Time history evolution of the average equivalent plastic strain within the off-fault bulk for three cases of different cohesion. Shading indicate partitioning between aseismic and coseismic plasticity. (d) The integrated equivalent plastic strain evolution with seismic potency indicating that complexity is associated with more bias toward off-fault deformations.

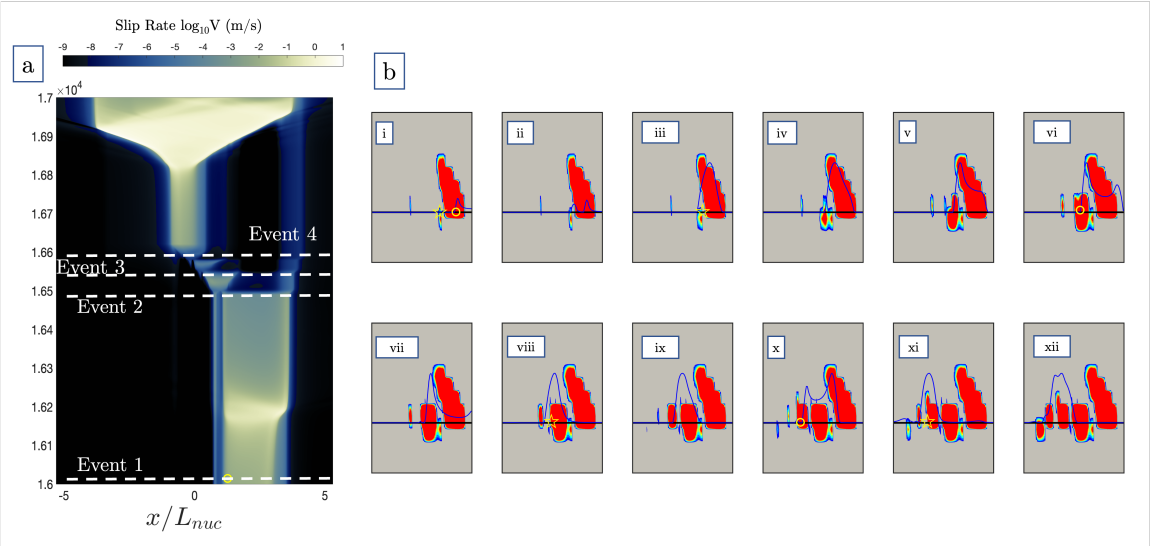

Figure 4: A specific snapshot for a cascading event presented for a case with cohesion $c = 30$ MPa. (a) The slip rate evolution for a viscoplastic 2-D fault illustrating cascading rupture propagation.(b) The partitioning between off-fault deformation and fault slip during this particular event sequence showing jerky rupture propagation in the form of individual events nucleation and arrest. The blue lines highlight the slip rate profile along the fault. The yellow circle indicate the location of rupture arrest, and the yellow start indicates the hypocenter of the renucleated rupture.

and aseismic phases also varies based on the choice of cohesion. As the cohesion decreases, a larger portion of overall plasticity accumulation is being accounted for aseismically. Specifically, by the end of the simulation, almost 19% of the total plastic strain is accumulated aseismically for $c = 30$ MPa. This fraction increased to 30% for $c = 22$ MPa. The increased role of aseismic plasticity partially explain the increased complexity in the seismicity and stress at lower bulk strength.

Finally, the partitioning of deformations between fault slip and off-fault plasticity plays a critical role in modulating the co-evolution of seismicity and fault zones. To highlight this, 3d shows the evolution of the integrated equivalent plastic strain within the near-fault region with fault slip expressed in terms of potency. There are two key observations: (1) the ratio between the integrated equivalent plastic strain and potency increases as the cohesion, and hence bulk strength, decreases, and (2) jumps associated with the increase in equivalent plastic strain are associated with minimal changes in potency. The first observation implies that complexity is proportional to the accumulation of plastic strain, with complexity being associated with more inelastic deformation delocalizing into the bulk. However, even for $c = 22$ MPa, the integrated equivalent plastic strain remain of the order of 1% of the seismic potency. The second observation suggests that there are periods during which it is more favorable for the deformation to be accommodated as bulk plastcity rather than fault slip. This, for example, may correspond to episodes of failed nucleation or arrested partial ruptures. In other words, these periods correspond to aseismic phases or episodes of transient slip deficit.

3.3 Cascading Earthquakes

Within our earthquake sequence with off-fault plasticity we observe the emergence of cascading earthquakes. These earthquakes just rupture, individually, a segment of the fault before arresting due to off-fault deformations. Nevertheless, due to a combination of (1) the favorable stress state and (2) the continuous creeping that concentrates the stress ahead of the pinned

rupture, subsequent earthquakes persistently nucleate along various segments of the fault in a brief timeframe, leading up to the eventual activation of the entire fault. Figure 4a shows the a cascading event sequence that occur for the case with cohesion $c = 30$ MPa. We observe the complexity of the earthquake sequence described above. Initially the rupture nucleates on the right side of the fault $x/L_{nuc} = 2.5$, the rupture propagate bilaterally prior to arresting due to inelastic strain accumulation. Eventually the stress concentration ahead of the pinned rupture tip is sufficient to trigger another rupture, which initiates ahead of the arrested event and rupture a new segment of the fault. This pattern keeps repeating with the triggering of event 3, and 4. Event 4 eventually rupture the whole seismogenic zone.

Figure 4c shows the rupture propagation as well as the pattern of plasticity accumulation within the bulk at different time steps within the cascading sequence of events. In panel (i-ii) We observe the onset of rupture arrest marked by the yellow circle accompanied by a substantial accumulation of off-fault plasticity. Within the same panel we highlight the location where the subsequent event will be triggered by a yellow star. The subsequent event is triggered ahead of the previously arrested panel as shown in panel (iii). In the intermediate panels (iii-v) the rupture proceeds to propagate prior to arresting in panel (vi) due to the accumulation of substantial inelastic strains. This pattern repeats again for the new ruptures that nucleates in panel (viii), and panel (xi).

This observed behavior is qualitatively similar to what has been observed in the quasi-static mode I fracture of elastic, perfectly plastic material in the plane strain configuration using the phase field approach[49]. Phase field models revealed that a plastic zone dulls the tip of a notch or crack, thereby impeding the initiation and spreading of the crack. When subjected to an adequate load, the crack initiates or unpins, but this occurs with a finite jump. As a result, the propagation is sporadic or abrupt, resulting in a rough surface. This jerky motion seems to persist for mode II dynamic fractures as observed here in our simulations suggesting a universal signature in elasto-plastic fracture phenomena.

4 Discussion

Our results indicate the accumulation of aseismic and coseismic off-fault deformation within the fault zone interact strongly with slip accumulation on the fault surface resulting in variations in the seismicity and stress patterns. In this work, we show that changing the bulk strength alters the earthquake sequence to produce complex slip patterns that depend on the extent of plastic strain accumulation. Based on the choice of bulk strength the fault surface exhibit a plethora of complex behavior such as partial ruptures, slow events, and intermittent episodes of earthquakes. The spatiotemporal complexity observed in our models is not tied to the particular choice of fault size[50], geometry[47] or heterogeneous distribution of frictional parameters. Rather, this complexity is attributed to the partitioning of deformation between fault slip and inelastic deformation in the bulk.

We have shown that plasticity accumulation produces persistent changes to the background stress field that influence the long term fault zone evolution and leads to emergence of regions of alternating compressive and tensile perturbations in the mean stress. Furthermore, our simulations highlight the role of bulk plasticity in the evolution of fault roughness and consequently short wavelength variations in the fault normal stress. These observations are consistent with recent experimental findings demonstrating that the sudden slip transition (in this particular case: the pinning of rupture tip) may produce substantial off-fault deformations and alter the fault surface in the fault normal direction [19].

Furthermore, we observe that the accumulation of off-fault inelastic deformations can lead to cascading sequence of events. This is due to accumulation of plastic zone which dulls the tip of the rupture front, thereby impeding the initiation and spreading of the rupture. Subjected to an sufficient load the rupture renucleate, however, with a finite jump. Consequently, the rupture

propagation becomes jerky, and within a short period of time (shorter than the recurrence interval) several segments of the fault rupture independently. We note here that in the presence of inelastic deformations we don't require any particular scaling of the fracture energy. Smaller events are a direct consequence of more plastic dissipation and prior slip history, which eliminate the need for fracture energy scaling (Gabriel et al., 2023) to achieve cascading events [51]. Furthermore, this study shows cascading events on a single fault that undergoes geometrical and stress state evolution due to off-fault plasticity over seismic cycles. This observation of cascading events is different from other cascading mechanisms involving elastic stress transfer in fault segments or a network of faults [52–54].

We note that we have not studied very low cohesion values due to numerical instabilities that emerge with the plasticity accumulation during the aseismic phases of the cycle prior to any coseismic activity. However, recent work by Mia et al 2023, for antiplane deformations reveals that as the rock strength is further reduced, the fault transitions into slow slip and seismicity eventually shut off[39]. This limit remains to be studied in the in-plane case where aseismic deformations can introduce mean stress perturbations and shift the yield envelope.

The main conclusions are summarized as follows:

1. Incorporating off-fault plasticity enable a transition from simple periodic through-going events for higher bulk strength to chaotic sequences that exhibit temporal clustering and spatial segmentation in the limit of lower bulk strength.

2. Accumulation of off-fault plasticity and emergence of partial ruptures lead to the evolution of spatially heterogeneous normal stress field on the fault surface with short wavelength variations, as well as, non-planar fault surface profile. For lower bulk strength, the fault surface develop shorter wavelength undulations.

3. The overall plastic strain increases with decreasing bulk strength. The fraction of plastic strain accumulated aseismically also increases with decreasing bulk strength.

4. The ratio between integrated plastic strain and potency increases with decreasing bulk strength suggesting that a key mechanism for complex evolution of seismicity and stress in fault zones lies in delocalizing of deformations. Lower bulk strength facilitates this delocalization.

5. The extent of the fault zone that is plastically deforming remains very small compared to the overall fault length. The ratio between the integrated plastic strain and potency is also below 1% even for the lowest cohesion value considered in this study. Nonetheless, the impact of bulk plasticity on seismicity and stresses is significant. This suggests the need for further high resolution studies to characterize the complex near-fault response.

6. Off-fault plasticity present a possible mechanism for generating cascading earthquakes without the need for fracture energy scaling. Cascading earthquakes and temporal clustering of earthquakes have been recently observed during the 2023 Herat earthquake sequence [55]

Acknowledgment

M.A. would like to thank Ares Rosakis for insightful discussions. M.A. also acknowledges support by the Caltech/MCE Big Ideas Fund (BIF), as well as the Caltech Terrestrial Hazard Observation and Reporting Center (THOR). The authors acknowledge support from the Southern California Earthquake Center through a collaborative agreement between NSF. Grant Number: EAR0529922 and USGS. Grant Number: 07HQAG0008 and the National Science Foundation CAREER award No. 1753249 for modeling complex fault zone structures. This material is based upon work supported by the Department of Energy under Award Number DE-FE0031685.

Data Availability

The authors accept AGU's data policy. Data generated from numerical simulations are uploaded on CALTECH DATA repository and available online at https://data.caltech.edu/records/nvvng-qsg61.

References

1. Chester, F. M., Evans, J. P. & Biegel, R. L. Internal structure and weakening mechanisms of the San Andreas Fault. *Journal of Geophysical Research: Solid Earth* **98,** 771–786. ISSN: 01480227. http://doi.wiley.com/10.1029/92JB01866 (Jan. 1993).
2. Mitchell, T. M. & Faulkner, D. R. The nature and origin of off-fault damage surrounding strike-slip fault zones with a wide range of displacements: A field study from the Atacama fault system, northern Chile. *Journal of Structural Geology* **31,** 802–816. ISSN: 01918141. http://dx.doi.org/10.1016/j.jsg.2009.05.002 (2009).
3. Huang, Y., Ampuero, J.-P. & Helmberger, D. V. Earthquake ruptures modulated by waves in damaged fault zones. *Journal of Geophysical Research: Solid Earth* **119,** 3133–3154. ISSN: 21699313. http://doi.wiley.com/10.1002/2013JB010724 (Apr. 2014).
4. Huang, Y., Beroza, G. C. & Ellsworth, W. L. Stress drop estimates of potentially induced earthquakes in the Guy-Greenbrier sequence. *Journal of Geophysical Research: Solid Earth* **121,** 6597–6607. ISSN: 21699313. http://doi.wiley.com/10.1002/2016JB013067 (Sept. 2016).
5. Barbot, S., Fialko, Y. & Sandwell, D. Effect of a compliant fault zone on the inferred earthquake slip distribution. *Journal of Geophysical Research: Solid Earth* **113,** 1–10. ISSN: 21699356 (2008).
6. Lewis, M. A. & Ben-Zion, Y. Diversity of fault zone damage and trapping structures in the Parkfield section of the San Andreas Fault from comprehensive analysis of near fault seismograms. *Geophysical Journal International* **183,** 1579–1595. ISSN: 0956540X. https://academic.oup.com/gji/article-lookup/doi/10.1111/j.1365-246X.2010.04816.x (Dec. 2010).
7. Y.-G. Li & Leary, P. C. Fault zone trapped seismic waves. *Bulletin of the Seismological Society of Americ* **80,** 1245–127 (1990).
8. Savage, H. M. & Brodsky, E. E. Collateral damage: Evolution with displacement of fracture distribution and secondary fault strands in fault damage zones. *Journal of Geophysical Research: Solid Earth* **116.** ISSN: 21699356 (Mar. 2011).
9. Biegel, R. L. & Sammis, C. G. *Relating Fault Mechanics to Fault Zone Structure* 2004.
10. Faulkner, D. R., Lewis, A. C. & Rutter, E. H. On the internal structure and mechanics of large strike-slip fault zones: Field observations of the Carboneras fault in southeastern Spain. *Tectonophysics* **367,** 235–251. ISSN: 00401951 (June 2003).
11. Weigandt, C., Griffith, W. & Rockwell, T. Role of confinement in coseismic pulverization: Testing the rock record of rupture directivity on the San Jacinto fault, Southern California. *Journal of Structural Geology* **177,** 104999. ISSN: 0191-8141. https://www.sciencedirect.com/science/article/pii/S019181412300216X (2023).
12. Huang, Y., Ampuero, J.-P. & Helmberger, D. V. Earthquake ruptures modulated by waves in damaged fault zones. *Journal of Geophysical Research: Solid Earth* **119,** 3133–3154. eprint: https://agupubs.onlinelibrary.wiley.com/doi/pdf/10.1002/2013JB010724. https://agupubs.onlinelibrary.wiley.com/doi/abs/10.1002/2013JB010724 (2014).

13. Smith, Z. D. & Griffith, W. A. Evolution of Pulverized Fault Zone Rocks by Dynamic Tensile Loading During Successive Earthquakes. *Geophysical Research Letters* **49.** e2022GL099971 2022GL099971, e2022GL099971. eprint: https://agupubs.onlinelibrary.wiley.com/doi/pdf/10.1029/2022GL099971. https://agupubs.onlinelibrary.wiley.com/doi/abs/10.1029/2022GL099971 (2022).

14. Ben-Zion, Y. & Ampuero, J.-P. Seismic radiation from regions sustaining material damage. *Geophysical Journal International* **178,** 1351–1356. ISSN: 0956-540X. eprint: https://academic.oup.com/gji/article-pdf/178/3/1351/5871906/178-3-1351.pdf. https://doi.org/10.1111/j.1365-246X.2009.04285.x (Sept. 2009).

15. Ben-Zion, Y. & Lyakhovsky, V. Representation of seismic sources sustaining changes of elastic moduli. *Geophysical Journal International* **217,** 135–139. ISSN: 0956-540X. eprint: https://academic.oup.com/gji/article-pdf/217/1/135/27662171/ggz018.pdf. https://doi.org/10.1093/gji/ggz018 (Jan. 2019).

16. Lyakhovsky, V. & Ben-Zion, Y. Isotropic seismic radiation from rock damage and dilatancy. *Geophysical Journal International* **222,** 449–460. ISSN: 0956-540X. eprint: https://academic.oup.com/gji/article-pdf/222/1/449/33181717/ggaa176.pdf. https://doi.org/10.1093/gji/ggaa176 (Apr. 2020).

17. Kwiatek, G. & Ben-Zion, Y. Assessment of P and S wave energy radiated from very small shear-tensile seismic events in a deep South African mine. *Journal of Geophysical Research: Solid Earth* **118,** 3630–3641. eprint: https://agupubs.onlinelibrary.wiley.com/doi/pdf/10.1002/jgrb.50274. https://agupubs.onlinelibrary.wiley.com/doi/abs/10.1002/jgrb.50274 (2013).

18. Cheng, Y., Wang, X., Zhan, Z. & Ben-Zion, Y. Isotropic Source Components of Events in the 2019 Ridgecrest, California, Earthquake Sequence. *Geophysical Research Letters* **48.** e2021GL094515 2021GL094515, e2021GL094515. eprint: https://agupubs.onlinelibrary.wiley.com/doi/pdf/10.1029/2021GL094515. https://agupubs.onlinelibrary.wiley.com/doi/abs/10.1029/2021GL094515 (2021).

19. Ross, E. O., Reber, J. E. & Titus, S. J. Relating Slip Behavior to Off-Fault Deformation Using Physical Models. *Geophysical Research Letters* **49.** ISSN: 0094-8276 (June 2022).

20. Ben-Zion, Y. & Sammis, C. G. Characterization of fault zones. *Pure and Applied Geophysics* **160,** 677–715. ISSN: 00334553 (2003).

21. Abdelmeguid, M. & Elbanna, A. Modeling Sequences of Earthquakes and Aseismic Slip (SEAS) in Elasto-Plastic Fault Zones With a Hybrid Finite Element Spectral Boundary Integral Scheme. *Journal of Geophysical Research: Solid Earth* **127.** e2022JB024548 2022JB024548, e2022JB024548. eprint: https://agupubs.onlinelibrary.wiley.com/doi/pdf/10.1029/2022JB024548. https://agupubs.onlinelibrary.wiley.com/doi/abs/10.1029/2022JB024548 (2022).

22. Rice, J. R., Sammis, C. G. & Parsons, R. Off-fault secondary failure induced by a dynamic slip pulse. *Bulletin of the Seismological Society of America* **95,** 109–134. ISSN: 00371106 (Feb. 2005).

23. Mitchell, T. M. & Faulkner, D. R. Towards quantifying the matrix permeability of fault damage zones in low porosity rocks. *Earth and Planetary Science Letters* **339-340,** 24–31. ISSN: 0012821X (July 2012).

24. Childs, C. *et al.* A geometric model of fault zone and fault rock thickness variations. *Journal of Structural Geology* **31,** 117–127. ISSN: 01918141 (Feb. 2009).

25. Heap, M. J., Faulkner, D. R., Meredith, P. G. & Vinciguerra, S. Elastic moduli evolution and accompanying stress changes with increasing crack damage: Implications for stress changes around fault zones and volcanoes during deformation. *Geophysical Journal International* **183,** 225–236. ISSN: 0956540X (Oct. 2010).

26. Chester, J. S., Chester, F. M. & Kronenberg, A. K. Fracture surface energy of the Punchbowl fault, San Andreas system. *Nature* **437,** 133–136. ISSN: 0028-0836. http://www.nature.com/articles/nature03942 (Sept. 2005).

27. Griffith, W. A., Nielsen, S., Di Toro, G. & Smith, S. A. Rough faults, distributed weakening, and off-fault deformation. *Journal of Geophysical Research: Solid Earth* **115.** ISSN: 21699356 (Aug. 2010).

28. Mutlu, O. & Pollard, D. D. On the patterns of wing cracks along an outcrop scale flaw: A numerical modeling approach using complementarity. *Journal of Geophysical Research: Solid Earth* **113.** ISSN: 21699356 (June 2008).

29. Manighetti, I., King, G. & Sammis, C. G. The role of off-fault damage in the evolution of normal faults. *Earth and Planetary Science Letters* **217,** 399–408. ISSN: 0012821X. https://linkinghub.elsevier.com/retrieve/pii/S0012821X03006010 (Jan. 2004).

30. Tal, Y. & Faulkner, D. The Effect of Fault Roughness and Earthquake Ruptures on the Evolution and Scaling of Fault Damage Zones. *Journal of Geophysical Research: Solid Earth* **127.** ISSN: 2169-9313 (Jan. 2022).

31. Perrin, C., Manighetti, I., Ampuero, J. P., Cappa, F. & Gaudemer, Y. Location of largest earthquake slip and fast rupture controlled by along-strike change in fault structural maturity due to fault growth. *Journal of Geophysical Research: Solid Earth* **121,** 3666–3685. ISSN: 21699356 (May 2016).

32. Faulkner, D. R., Mitchell, T. M., Jensen, E. & Cembrano, J. Scaling of fault damage zones with displacement and the implications for fault growth processes. *Journal of Geophysical Research: Solid Earth* **116.** ISSN: 21699356 (May 2011).

33. Anders, M. H. & Wiltschko, D. V. *Microfracturing, paleostress and the growth of faults* tech. rep. 6 (1994), 795.

34. Dunham, E. M., Belanger, D., Cong, L. & Kozdon, J. E. Earthquake ruptures with strongly rate-weakening friction and off-fault plasticity, part 1: Planar faults. *Bulletin of the Seismological Society of America* **101,** 2296–2307. ISSN: 00371106 (2011).

35. Huang, Y. & Ampuero, J.-P. Pulse-like ruptures induced by low-velocity fault zones. *Journal of Geophysical Research* **116,** B12307. ISSN: 0148-0227. http://doi.wiley.com/10.1029/2011JB008684 (Dec. 2011).

36. Thakur, P., Huang, Y. & Kaneko, Y. Effects of Low-Velocity Fault Damage Zones on Long-Term Earthquake Behaviors on Mature Strike-Slip Faults. *Journal of Geophysical Research: Solid Earth* **125,** 1–20. ISSN: 21699356 (2020).

37. Erickson, B. A., Dunham, E. M. & Khosravifar, A. A finite difference method for off-fault plasticity throughout the earthquake cycle. *Journal of the Mechanics and Physics of Solids* **109,** 50–77. ISSN: 00225096. http://dx.doi.org/10.1016/j.jmps.2017.08.002 (2017).

38. Mia, M. S., Abdelmeguid, M. & Elbanna, A. E. Spatio-Temporal Clustering of Seismicity Enabled by Off-Fault Plasticity. *Geophysical Research Letters* **49.** ISSN: 19448007 (Apr. 2022).

39. Mia, M. S., Abdelmeguid, M. & Elbanna, A. E. The spectrum of fault slip in elastoplastic fault zones. *Earth and Planetary Science Letters* **619,** 118310. ISSN: 0012-821X. https://www.sciencedirect.com/science/article/pii/S0012821X23003230 (2023).

40. Cochard, A. & Rice, J. R. Fault rupture between dissimilar materials: Ill-posedness, regularization, and slip-pulse response. *Journal of Geophysical Research: Solid Earth* **105,** 25891–25907. ISSN: 01480227. http://doi.wiley.com/10.1029/2000JB900230 (Nov. 2000).

41. Ranjith, K. & Rice, J. R. *Slip dynamics at an interface between dissimilar materials* tech. rep. (2001), 341–361. www.elsevier.com/locate/jmps.

42. Tal, Y., Rubino, V., Rosakis, A. J. & Lapusta, N. Illuminating the physics of dynamic friction through laboratory earthquakes on thrust faults. *Proceedings of the National Academy of Sciences* **117,** 21095–21100. ISSN: 0027-8424. http://www.pnas.org/lookup/doi/10.1073/pnas.2004590117 (Sept. 2020).

43. Abdelmeguid, M., Ma, X. & Elbanna, A. A Novel Hybrid Finite Element-Spectral Boundary Integral Scheme for Modeling Earthquake Cycles: Application to Rate and State Faults With Low-Velocity Zones. *Journal of Geophysical Research: Solid Earth* **124,** 12854–12881. ISSN: 21699356 (Dec. 2019).

44. Templeton, E. L. & Rice, J. R. Off-fault plasticity and earthquake rupture dynamics: 1. Dry materials or neglect of fluid pressure changes. *Journal of Geophysical Research: Solid Earth* **113,** 1–19. ISSN: 21699356 (2008).

45. Abdelmeguid, M. & Elbanna, A. Modeling Sequences of Earthquakes and Aseismic Slip (SEAS) in Elasto-plastic Fault Zones with A Hybrid Finite Element Spectral Boundary Integral scheme. https://doi.org/10.1002/essoar.10511050.2.

46. Renard, F. & Candela, T. in *Fault Zone Dynamic Processes* 195–215 (American Geophysical Union (AGU), 2017). ISBN: 9781119156895. eprint: https://agupubs.onlinelibrary.wiley.com/doi/pdf/10.1002/9781119156895.ch10. https://agupubs.onlinelibrary.wiley.com/doi/abs/10.1002/9781119156895.ch10.

47. Cattania, C. & Segall, P. Precursory Slow Slip and Foreshocks on Rough Faults. *Journal of Geophysical Research: Solid Earth* **126.** ISSN: 21699356 (Apr. 2021).

48. Romanet, P. & Ozawa, S. Fully Dynamic Earthquake Cycle Simulations on a Nonplanar Fault Using the Spectral Boundary Integral Element Method (sBIEM). *Bulletin of the Seismological Society of America* **112,** 78–97. ISSN: 0037-1106. eprint: https://pubs.geoscienceworld.org/ssa/bssa/article-pdf/112/1/78/5518864/bssa-2021178.1.pdf. https://doi.org/10.1785/0120210178 (Oct. 2021).

49. Brach, S., Tanné, E., Bourdin, B. & Bhattacharya, K. Phase-field study of crack nucleation and propagation in elastic–perfectly plastic bodies. *Computer Methods in Applied Mechanics and Engineering* **353,** 44–65. ISSN: 0045-7825. https://www.sciencedirect.com/science/article/pii/S0045782519302300 (2019).

50. Barbot, S. Modulation of fault strength during the seismic cycle by grain-size evolution around contact junctions. *Tectonophysics* **765,** 129–145. ISSN: 00401951. https://doi.org/10.1016/j.tecto.2019.05.004 (2019).

51. Gabriel, A.-A., Garagash, D. I., Palgunadi, K. H. & Mai, P. M. *Fault-size dependent fracture energy explains multi-scale seismicity and cascading earthquakes* 2023. arXiv: 2307.15201 [physics.geo-ph].

52. Palgunadi, K. H., Gabriel, A.-A., Garagash, D. I., Ulrich, T. & Mai, P. M. *Rupture Dynamics of Cascading Earthquakes in a Multiscale Fracture Network* 2023. arXiv: 2307.14229 [physics.geo-ph].

53. Im, K. & Avouac, J.-P. Cascading foreshocks, aftershocks and earthquake swarms in a discrete fault network. *Geophysical Journal International* **235,** 831–852. ISSN: 0956-540X. eprint: https://academic.oup.com/gji/article-pdf/235/1/831/50959708/ggad278.pdf. https://doi.org/10.1093/gji/ggad278 (July 2023).

562 54. Ozawa, S. & Ando, R. Mainshock and Aftershock Sequence Simulation in Geometrically
563 Complex Fault Zones. *Journal of Geophysical Research: Solid Earth* **126.** e2020JB020865
564 2020JB020865, e2020JB020865. eprint: https://agupubs.onlinelibrary.wiley.com/
565 doi/pdf/10.1029/2020JB020865. https://agupubs.onlinelibrary.wiley.com/doi/
566 abs/10.1029/2020JB020865 (2021).
567 55. US Geological Survey. *M 6.3 - 34 km NNW of Herāt, Afghanistan* https://earthquake.
568 usgs.gov/earthquakes/eventpage/us6000lfn5/executive.

Appendix A Model Setup

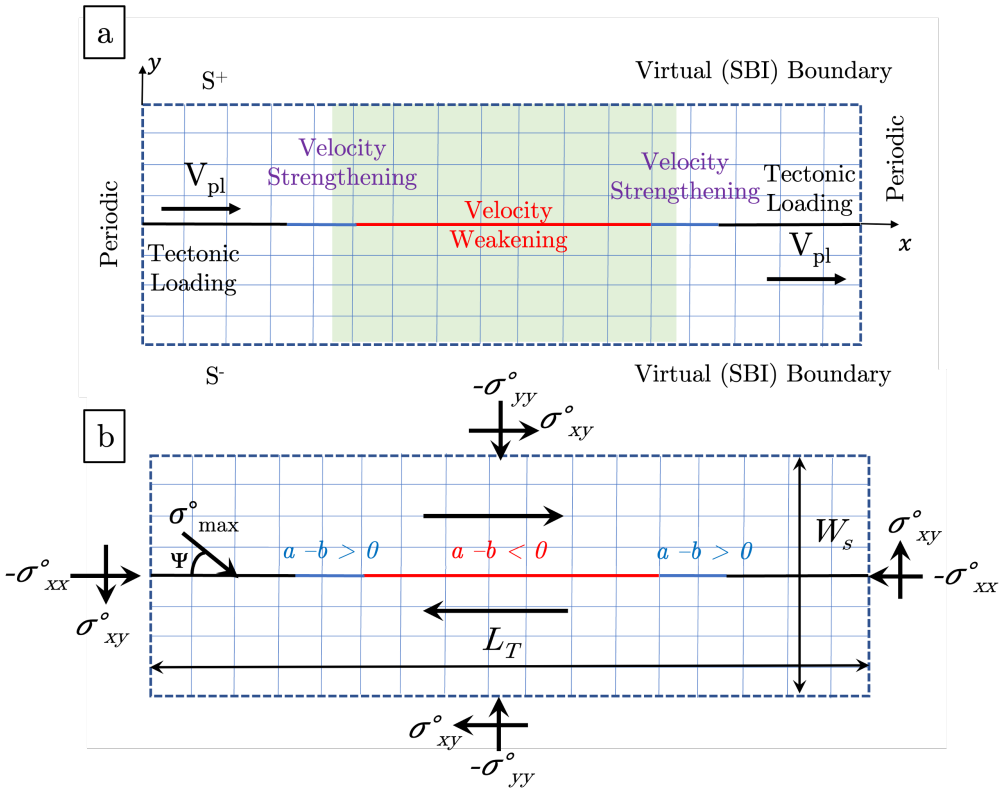

Figure A1: **Schematic of the model considered in this paper** (a) The computational setup for the hybrid FE-SBI scheme. A domain Ω adjacent to the fault surface is discretized using the finite element method. The spectral boundary integral method is utilized to model the external linearly elastic half spaces without explicit discretization. The response on the virtual boundaries parallel to the fault surface is expressed through an integral relation between the displacement and traction. Periodicity is imposed on the lateral boundaries of the domain. (b) The distribution of the fault frictional parameters and background tectonic stress field.

Table A1: Parameters description

Medium Parameter	Symbol	Value
Shear wave speed (km/s)	c_s	3.5
Pressure wave speed (km/s)	c_p	6.0
Density (kg/m^3)	ρ	2670.0
Length of the domain (m)	L_T	150
Distance between two virtual boundaries (m)	W_s	varies
Angle of Internal Friction	ϕ	31.6°
Cohesion MPa	c	varies
Angle of Maximum Compressive principal stress	Ψ	45°
Viscosity term (MPa-s)	η	0.32
Background Stress	**Symbol**	**Value**
Background Vertical Stress MPa	σ_{yy}	120
Background Horizontal Stress MPa	σ_{xx}	120
Background Shear Stress MPa	σ_{xy}	59.1
Fault Parameters	**Symbol**	**Value**
Static Coefficient of friction	f_o	0.6
Critical slip distance (μm)	L	50
Reference velocity (m/s)	V_o	10^{-6}
Tectonic loading (m/s)	V_{pl}	10^{-9}
Length of VW patch (m)	L_{VW}	50
Length of transition (m)	L_{VW-VS}	5
Length of the fault (m)	L_f	90
Evolution effect parameter	b	0.015
Steady state velocity dependence in VW patch	$(a_{VW} - b)$	-0.005
Steady state velocity dependence in VS patch	$(a_{VS} - b)$	0.015
Nucleation size (m)	L_{nuc}	6.96
Quasi-static process zone size (m)	L_b	1.2
Grid size (m)	$\triangle x$	0.1